

Visible transparent *β*-Ga_2O_3 solar-blind UV high-performance photodetector for stable high-temperature operation

Chao Zhang(张超), Jinpeng Dong(董瑾鹏), Gang Li(李刚), Yida Guan(管艺达), Jiahao Zhang(张嘉豪), Qingyu Wang(王清玉), Zhilin Wang(王志林), Duo Sun(孙多), Yue Sun(孙悦), and Lili Wang(王丽丽)
Citation: Chin. Phys. B, 2026, 35 (**5**): 056106. DOI: 10.1088/1674-1056/ae311f
http://cpb.iphy.ac.cn; http://iopscience.iop.org/cpb

What follows is a list of articles you may be interested in

Pressure-induced amorphization and metallization in orthorhombic SiP

Qiru Zeng(曾琪茹), Youjun Zhang(张友君), Yukai Zhuang(庄毓凯), Linfei Yang(杨林飞), Qiming Wang(王齐明), and Yi Sun(孙熠)
Chin. Phys. B, 2025, 34 (**9**): 096102. DOI: 10.1088/1674-1056/add4f6

Synergistic improvements in mechanical and thermal performance of TiB_2 solid-solution-based composites

Zhuang Li(李壮), Cun You(由存), Zhihui Li(李志慧), Xuepeng Li(李雪鹏), Guiqian Sun(孙贵乾), Xinglin Wang(王星淋), Qi Jia(贾琪), Qiang Tao(陶强), and Pinwen Zhu(朱品文)
Chin. Phys. B, 2025, 34 (**8**): 086105. DOI: 10.1088/1674-1056/add00c

Light trapping and optical absorption enhancement in vertical semiconductor Si/SiO_2 nanowire arrays

Ying Wang(王莹), Xin-Hua Li(李新化)
Chin. Phys. B, 2018, 27 (**2**): 026102. DOI: 10.1088/1674-1056/27/2/026102

Large scale silver nanowires network fabricated by MeV hydrogen (H^+) ion beam irradiation

Honey S, Naseem S, Ishaq A, Maaza M, Bhatti M T, Wan D
Chin. Phys. B, 2016, 25 (**4**): 046105. DOI: 10.1088/1674-1056/25/4/046105

A new family of sp^3-hybridized carbon phases

Ning Xu(徐宁), Jian-Fu Li(李建福), Bo-Long Huang(黄勃龙), Bao-Lin Wang(王保林)
Chin. Phys. B, 2016, 25 (**1**): 016103. DOI: 10.1088/1674-1056/25/1/016103

Visible transparent β-Ga_2O_3 solar-blind UV high-performance photodetector for stable high-temperature operation

Chao Zhang(张超)[1,†], Jinpeng Dong(董瑾鹏)[1], Gang Li(李刚)[1], Yida Guan(管艺达)[2], Jiahao Zhang(张嘉豪)[1], Qingyu Wang(王清玉)[1], Zhilin Wang(王志林)[1], Duo Sun(孙多)[1], Yue Sun(孙悦)[1], and Lili Wang(王丽丽)[1,‡]

[1] *Key Laboratory of Advanced Structural Materials, Ministry of Education, and School of Materials Science and Engineering, Changchun University of Technology, Changchun* 130012, *China*

[2] *College of Electrical and Computer Engineering, Jilin Jianzhu University, Changchun* 130118, *China*

(Received 28 October 2025; revised manuscript received 11 December 2025; accepted manuscript online 25 December 2025)

Transparent ultraviolet (UV) photodetectors have garnered significant interest due to their promising applications in integrated transparent electronics. In this work, a visible transparent solar-blind ultraviolet photodetector with stable crystalline ITO electrodes based on a β-Ga_2O_3 film has been fabricated and characterized from room temperature to 400 °C. The results demonstrate that the device maintains excellent thermal stability even at high temperatures up to 400 °C and achieves outstanding performance metrics, including a low dark current of 7.5 pA, a superb UV/visible rejection ratio of 7.8×10^5, and a large detectivity of 1.3×10^{15} Jones. This overall performance surpasses that of most other reported Ga_2O_3-based transparent UV photodetectors. Therefore, the fabricated high-performance transparent β-Ga_2O_3 solar-blind UV photodetector demonstrates considerable potential for applications in advanced transparent electronics under extreme environments.

Keywords: solar-blind UV detector, Ga_2O_3 film, transparent, high temperature

PACS: 61.72.uj, 61.80.Ba, 73.61.Ga, 85.60.Gz

DOI: 10.1088/1674-1056/ae311f **CSTR:** 32038.14.CPB.ae311f

1. Introduction

In recent years, solar-blind ultraviolet (UV) photodetectors have garnered considerable interest in various fields, including fire detection, missile warning, space communication, and environmental monitoring.[1–4] Until now, several kinds of wide-bandgap semiconductor materials, such as diamond, ZnMgO, AlGaN, and Ga_2O_3, have been used to demonstrate UV photodetectors.[5–9] Among these materials, Ga_2O_3 is considered an auspicious material for solar-blind UV photodetection due to its superior properties, including a suitable direct bandgap, high radiation hardness, excellent chemical inertness, and thermal stability.[10–13] There are six different crystalline structures of Ga_2O_3, and the most stable phase among them is monoclinic β-Ga_2O_3.[14–16] To date, various types of photodetector structures based on Ga_2O_3 materials, such as metal–semiconductor–metal (MSM), Schottky, and heterojunction, have been demonstrated.[17–19] Among them, MSM-type photodetectors are widely employed, benefiting from their fast response speed, straightforward fabrication process, and ease of integration.[20–23] For many extreme environmental applications, such as flame detection with high surface temperatures, ultraviolet photodetectors that are capable of operating at high temperatures are highly desirable. Consequently, the operating temperature of solar-blind photodetectors should be increased further to meet the requirements of extreme environments. However, there are some reports about Ga_2O_3-based high-temperature solar-blind photodetectors, which prove that Ga_2O_3 is a promising material for high-temperature applications due to its superior thermal conductivity.[24–26] Nevertheless, the development of solar-blind ultraviolet photodetectors based on Ga_2O_3 thin films for extreme environments remains at an early stage, and their performance still falls short of expectations. Recently, transparent electronics have emerged as a promising technology for next-generation optoelectronic devices, which have been fabricated for various applications.[27–30] Transparent UV photodetectors are crucial for enabling integrated transparent electronics, including displays, bright windows, batteries, and so on.[31–33] Therefore, visible transparent photodetectors consisting of transparent electrodes and wide-bandgap semiconductors are indispensable for the integration toward transparent electronics. So far, multiple reports have detailed Ga_2O_3-based MSM photodetectors that utilize transparent electrodes. For example, Kumar *et al.* reported a transparent, flexible, and high-performance amorphous Ga_2O_3 solar-blind photodetector incorporating amorphous IZO electrodes. This device demonstrated higher responsivity and external quantum efficiency compared to conventional Ag metal electrodes.[34] Sui *et al.* reported a flexible transparent Ga_2O_3 solar-blind ultraviolet photodetector fabricated on a mica substrate with indium

†Corresponding author. E-mail: zhangchao@ccut.edu.cn

‡Corresponding author. E-mail: wanglili@ccut.edu.cn

© 2026 Chinese Physical Society and IOP Publishing Ltd. All rights, including for text and data mining, AI training, and similar technologies, are reserved.

tin oxide (ITO) electrodes. Compared to a room-temperature-fabricated photodetector, the flexible device on mica exhibits improved solar-blind UV photoresponse characteristics.[35] Unfortunately, most reported transparent Ga_2O_3 solar-blind photodetectors are based on amorphous Ga_2O_3 films and amorphous electrode materials, which limit their application in extreme environments, such as high temperatures. High-temperature environments can cause crystallization changes in amorphous Ga_2O_3 films and electrode materials, which can impact the performance and stability of photodetectors. Therefore, a critical challenge lies in further increasing their operational temperature to meet the practical requirements of extreme conditions, such as sustained high-temperature environments.

In our work, β-Ga_2O_3 thin films were grown using metal–organic chemical vapor deposition technology on c-Al_2O_3 substrates, followed by a high-temperature postannealing at 750 °C. Annealed crystallized ITO electrodes on β-Ga_2O_3 films are prepared by magnetron sputtering. Transparent Ga_2O_3-based MSM solar-blind UV photodetectors with ITO transparent electrodes were constructed. The as-fabricated photodetector exhibits better performance compared to the photodetector with conventional Au electrodes. Moreover, the performance of the photodetector featuring crystalline ITO transparent electrodes was evaluated across a broad temperature range of 25 °C to 400 °C, demonstrating its exceptional stability and reliability.

2. Experimental details

The β-Ga_2O_3 thin films were grown on c-Al_2O_3 substrates by metal−organic chemical vapor deposition (MOCVD). The growth was carried out at 700 °C under a chamber pressure of 9.5×10^2 Pa. Triethylgallium (TEGa) and high-purity oxygen were employed as the precursors, with high-purity nitrogen serving as the carrier gas. The flow rates were set at 5 sccm and 500 sccm for TEGa and oxygen, respectively. Subsequently, the sample underwent thermal annealing at 750 °C for 60 minutes in a pure oxygen atmosphere within a horizontal tube furnace. The ITO interdigital electrodes (50 nm thick) were fabricated on β-Ga_2O_3 films using photolithography & lift-off techniques. The ITO film was deposited via magnetron sputtering for 30 minutes. The deposition was carried out in a gas mixture of argon (20 sccm) and oxygen (5 sccm) at a working pressure of 1.1 Pa, with a sputtering power of 100 W. The ITO fingers are $\sim$ 10 μm in width and 500 μm in length, with a spacing of $\sim$ 10 μm. The ITO interdigital electrodes were subsequently annealed at 750 °C in an oxygen atmosphere for 40 minutes to achieve low resistance and a crystalline phase. Figure 1 illustrates the schematic fabrication process of the visible transparent β-Ga_2O_3 MSM photodetector. The surface of the films was evaluated using scanning electron microscopy (SEM) (Hitachi S-4800), and their structural properties were characterized by x-ray diffraction (XRD) (Cu-$K\alpha$ radiation, $\lambda = 0.154$ nm). The current–voltage (I–V) properties and time-dependent photocurrent (I–t) curves were measured by a semiconductor parameter analyzer (Agilent B1500A) at room temperature. Transmission spectra were recorded using a Shimadzu UV-3101PC spectrophotometer. The spectral response properties were obtained by using a 200 W UV enhanced Xe lamp and a monochromator.

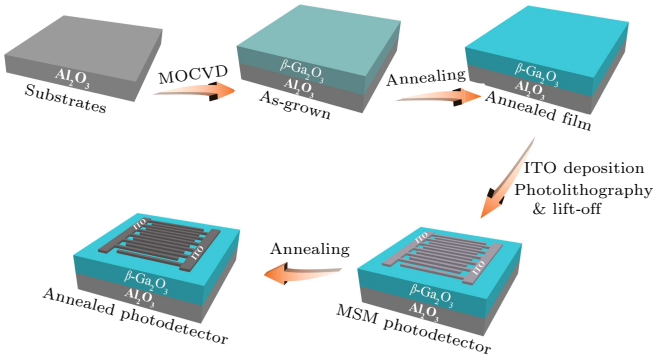


Fig. 1. Schematic of the fabrication process for the visible-transparent β-Ga_2O_3 MSM photodetector.

3. Results and discussion

The XRD pattern of the β-Ga_2O_3 film on a sapphire substrate was obtained further to investigate the monoclinic structure of the thin film. As shown in Fig. 2(a), the three observed diffraction peaks, located at 18.8°, 38.2°, and 58.9°, can be assigned to the (-201), (-402), and (-603) crystallographic planes of β-Ga_2O_3, respectively (JCPDS:43-1012). Figure 2(b) shows the XRD patterns of the ITO films on sapphire substrate before and after thermal annealing. Obviously, no discernible ITO diffraction peaks were observed in the as-grown films on the sapphire substrate, indicating an amorphous structure. In contrast, thermal annealing induced a transition to a more stable crystalline phase, as evidenced by the emergence of distinct diffraction peaks. This enhanced stability of films prevents performance degradation from phase changes in high-temperature environments, which is crucial for the application of ITO films as transparent electrodes.

Additionally, the SEM images of the transparent photodetector are presented in Figs. 2(c) and 2(d). The image of the photodetector's magnified electrode region is shown in Fig. 2(c). The device can be clearly observed, and the ITO finger electrodes have been well prepared on the β-Ga_2O_3 film. As shown in the images of Fig. 2(d), both annealed films exhibit considerably smooth surface morphology. The β-Ga_2O_3 film and the ITO electrodes have thicknesses of approximately 150 nm and 50 nm, respectively.

Figure 3(a) presents the optical transmission spectrum of the β-Ga_2O_3 thin film on a sapphire substrate, revealing a

high average transmittance of over 90% in the visible range (400–700 nm) and a steep absorption edge near 250 nm. The bandgap of the β-Ga_2O_3 thin film is $\sim$ 4.9 eV, which is calculated by extrapolating the linear region of the plot $(\alpha h\nu)^2$ versus $h\nu$ shown in the inset. The estimated bandgap is consistent with the values reported in the literature.[36,37] Furthermore, as shown in Fig. 3(b), the ITO film fabricated on the β-Ga_2O_3 thin film also exhibits a transmittance of over 80% throughout the visible band. Clearly, the high transmittance of both β-Ga_2O_3 and ITO films within the visible spectrum fulfills the critical requirement for optical transparency, rendering them highly suitable for transparent UV photodetectors. This transparency is directly evident in the device photograph inset in Fig. 3(b).

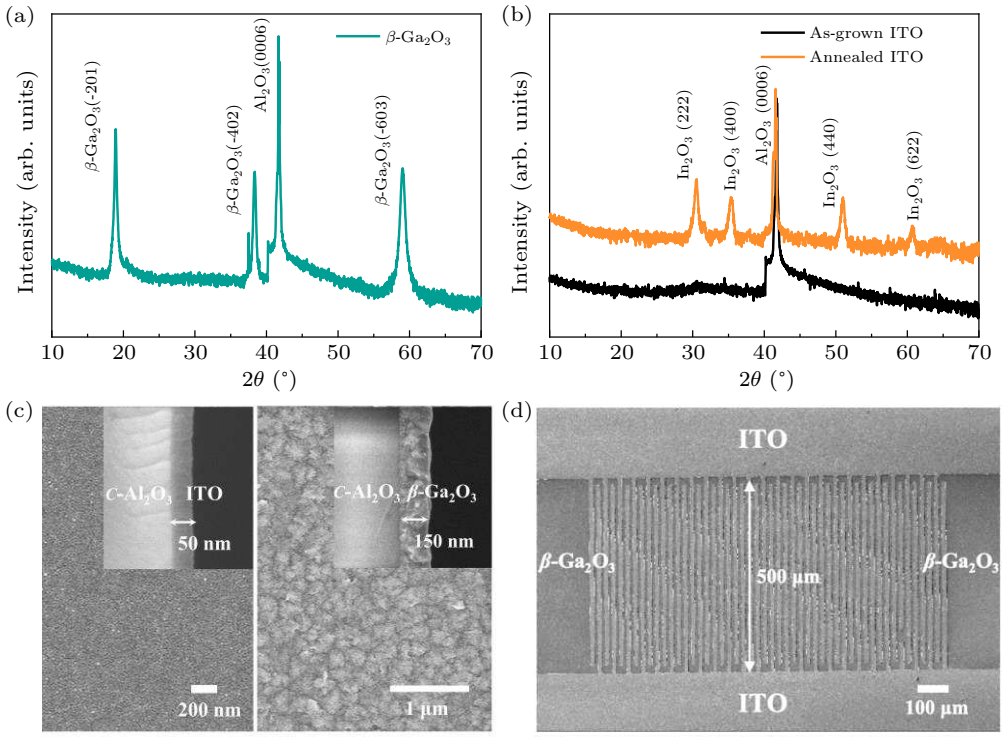


Fig. 2. XRD patterns of (a) the epitaxial β-Ga_2O_3 films and (b) ITO films on sapphire substrates before and after thermal annealing. SEM images of (c) the β-Ga_2O_3 and ITO films (d) the ITO electrodes on the photodetector.

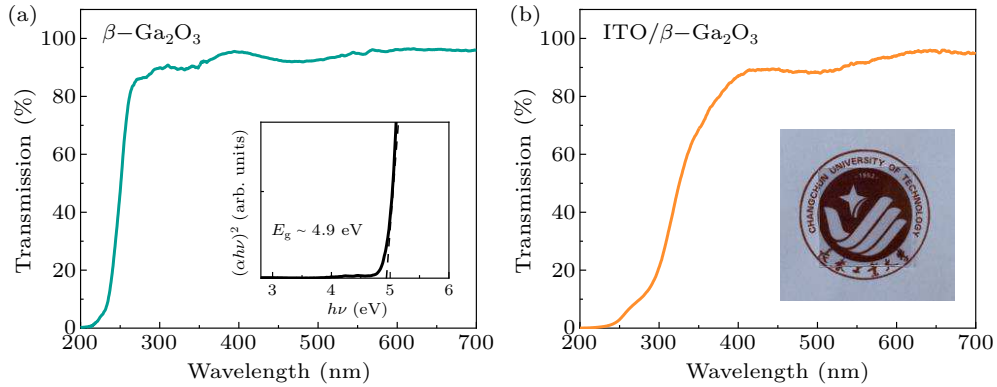


Fig. 3. Optical transmission spectra of (a) the β-Ga_2O_3 film and (b) the ITO on β-Ga_2O_3 film. The insets in panels (a) and (b) show the Tauc plot of the β-Ga_2O_3 film and an optical photograph of the photodetector, respectively.

Subsequently, β-Ga_2O_3-based solar-blind UV photodetectors with different electrodes were fabricated, and their performance was investigated at room temperature (25 °C). The schematic diagram of the measurement system is illustrated in Fig. 4(a), wherein the photodetector is connected to a semiconductor parameter analyzer. To investigate the electrical and optoelectrical properties of the device, *I*–*V* characteristics were measured on the photodetectors in the dark and under illumination at 254 nm with an intensity of $\sim$ 0.8 mW/cm². As clearly shown in Fig. 4(b), the dark currents of the two photodetectors fabricated with annealed films are significantly lower than those of the as-grown β-Ga_2O_3 film, which may be associated with the repair of defects in the films during thermal annealing. The photodetector with crystalline ITO electrodes exhibits an ultra-low dark current of 7.5 pA at 10 V. This low background noise enables the transparent device to detect

weak optical signals with exceptional ability by minimizing noise interference. The normalized photo-to-dark current ratio (NPDR) is an objective parameter for evaluation, which can avoid the effect of input light intensity. A higher ratio indicates the device's ability to generate a stronger photocurrent signal in the presence of the same level of dark current noise. It can be calculated using the following formula:[38,39]

$$\mathrm{NPDR} = \frac{I_{\mathrm{photo}}/I_{\mathrm{dark}}}{P_\lambda S},$$

where I_{photo} is the photocurrent, I_{dark} is the dark current, S is the effective illumination area of the device, and P_λ is the power density of the illumination light. The NPDR is as high as 2.9×10^{13} W^{-1}, which indicates the excellent photoelectric performance of the photodetector. Another figure of merit for photodetectors is the linear dynamic range (LDR) or photosensitivity linearity, typically quoted in decibels (dB). The following formula gives LDR:

$$\mathrm{LDR} = 20\log\frac{J^*_{\mathrm{ph}}}{J_{\mathrm{dark}}},$$

where J^*_{ph} is the photocurrent measured at a light intensity of 1 mW/cm^2. The transparent photodetector with ITO electrodes exhibits an LDR exceeding 100 dB at room temperature, demonstrating its excellent linear response over a wide range of light intensities.[40] The superb performance of the ITO-based transparent photodetector is ascribed to the high crystallization quality of films and the modification of the interface states.[41,42] Figure 4(d) presents the measured transient photocurrent (I–t) under 254 nm illumination at a bias of 10 V. When the light source is activated, photoexcitation in the Ga_2O_3 film produces electron–hole pairs. Under the influence of an external electric field, these carriers are separated and collected at the electrodes, resulting in a photocurrent. Following the initial response, the photocurrent tends to stabilize with prolonged illumination time. Obviously, all the photodetectors demonstrate a fast response and excellent reproducibility to periodic light pulses, indicating their superior ability to track UV signals. The photocurrents of all devices are comparable in magnitude. Besides, the 90% to 10% decay times of the devices were determined to be approximately 1 s, 0.5 s, and 0.2 s, respectively. Notably, the results indicate that the photodetector using ITO as electrodes exhibits faster response speed, enhancing the UV detection sensitivity and efficiency of the photodetector. Figure 4(e) presents the current-time curves of the ITO-based photodetector under 254 nm illumination of various intensities at 10 V. As the light intensity increases, the device's current under light irradiation increases significantly, exhibiting good stability and repeatability. Generally, photocurrent (I_{photo}) versus power density (P) is fitted using the following simple equation:[14,43]

$$I_{\mathrm{photo}} = AP^\theta,$$

where A is a constant, and θ is an exponent related to the trap states of the photodetector. The θ value was estimated to be ~ 0.87 by fitting the data, which is smaller than 1 (indicating an ideal trap-free device), suggesting the existence of low trap states in the transparent photodetector. The corresponding response time was investigated to evaluate the detection speed,

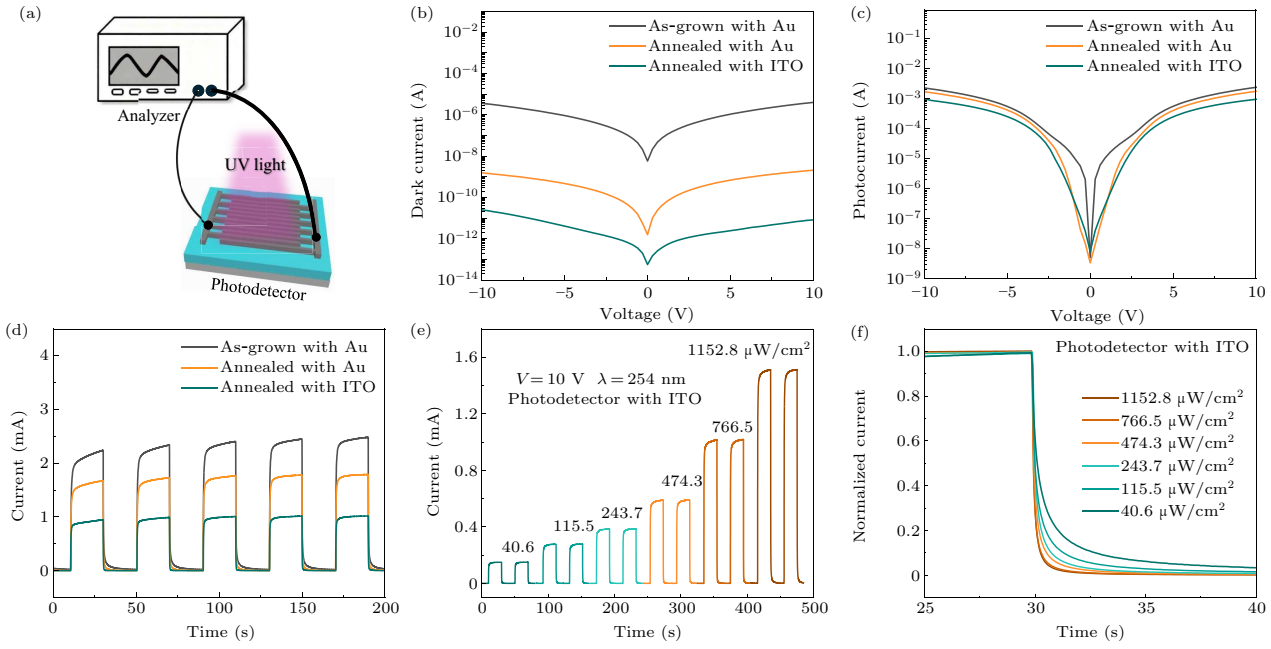


Fig. 4. (a) Schematic diagram of the testing system configuration. Semilogarithmic current–voltage characteristics of the photodetectors with different electrodes (b) in the dark and (c) under illumination (254 nm). (d) Time-dependent photoresponse with 254 nm light periodically on and off at 10 V. (e) Time-dependent photoresponse and (f) normalized response of the ITO-based photodetector under 254 nm illumination with different intensities, measured at a bias of 10 V.

Table 1. Performance comparison of our device and other Ga_2O_3 thin-film MSM transparent photodetectors.

Materials	Electrodes	Responsivity (A/W)	Dark current (A)	Rejection ratio	Detectivity (Jones)	Ref.
a-Ga_2O_3	AZO	2.66@10 V	2.84×10^{12}@10 V	$2.93\times10^{5}(R_{250}/R_{365})$	4.84×10^{14}	[45]
a-Ga_2O_3	IZO	43.99@2 V	11×10^{9}@5 V	$714.2(R_{250}/R_{555})$	–	[34]
a-Ga_2O_3	IZO	3.2×10^{-4}@10 V	$\sim1\times10^{9}$@200 V	–	2.8×10^{10}	[26]
a-Ga_2O_3	ITO	0.19@20 V	–	–	–	[46]
β-Ga_2O_3	ITO	–	6×10^{13}@10 V	$6.83\times10^{3}(R_{250}/R_{400})$	–	[35]
β-Ga_2O_3	AZO	1.25@5 V	1.5×10^{9}@5 V	–	–	[47]
β-Ga_2O_3	ITO	27.3@10 V	7.5×10^{-12}@10 V	$7.8\times10^{5}(R_{250}/R_{400})$	1.3×10^{15}	this work

as shown in Fig. 4(f). Clearly, the decay time exhibits a decreasing trend with increasing optical power density, indicating a faster photoresponse speed at higher illumination levels. This phenomenon is attributed to the formation of a thermal non-equilibrium state within the semiconductor upon exposure to light. An increase in light intensity elevates the number of generation–recombination centers, with the corresponding rate being proportional to the density of excess carriers produced by photoexcitation.[24,44]

Furthermore, the performance parameters of our work and recently reported transparent MSM photodetectors based on Ga_2O_3 thin films are listed in Table 1. Obviously, the UV/visible rejection ratio, dark current, and detectivity of our transparent photodetector at 25 °C are comparable to those of other transparent photodetectors based on Ga_2O_3 thin films.

To explore the potential of transparent photodetectors based on β-Ga_2O_3 films in elevated temperature applications, the device's performance is investigated at various temperatures. The I–V characteristic curves of the device were measured at various temperatures, as shown in Figs. 5(a) and 5(b). Although the dark current of the device increases with temperature, it remains at a low level of 100 pA at an elevated temperature of 400 °C under a 10 V bias. The rise in dark current can be attributed to thermal excitation. In this process, increased temperatures facilitate the excitation of more charge carriers into the conduction band, which in turn gives rise to a higher dark current. This performance demonstrates the capability of the device to detect weak signals in extreme environments (such as high temperatures). Similarly, the photocurrent shows a slight increase with temperature under illumination. The transient response (I–t) of the device was characterized by periodically switching the 254 nm lamp on and off at various temperatures under a constant 10 V bias. As shown in Fig. 5(c), the transparent photodetector demonstrates excellent thermal stability and repeatability at both room and high temperatures, which is attributed to the high thermal conductivity of the β-Ga_2O_3 film and the stable crystalline structure of the ITO transparent electrodes after thermal annealing. This performance contrasts with that of most reported transparent MSM photodetectors based on Ga_2O_3, which primarily utilize amorphous films and electrodes, and therefore lack stable high-temperature operation. Thus, as an alternative electrode material for current Ga_2O_3-based high-temperature photodetectors, crystalline ITO demonstrates superior performance in terms of high-temperature chemical inertness and interface stability, thereby reducing issues such as electrode oxidation and thermal mismatch.

Figure 5(d) depicts the spectral response of the device, presented on a semilogarithmic scale, over the wavelength range of 200–500 nm under a 10 V bias. Clearly, all the photodetectors exhibit a sharp spectral cut-off of −3 dB at $\sim$ 260 nm under both temperature conditions. The peak responsivity levels of the devices at 25 °C and 400 °C, at a wavelength of approximately 250 nm, were as high as $\sim$ 27.3 A/W and $\sim$ 35.5 A/W, respectively. Typically, the UV-to-visible rejection ratio is a key metric for evaluating the spectral selectivity of the photodetector, which is defined as the ratio between the peak responsivity and responsivity at 400 nm ($R_{\rm peak}/R_{400}$). The rejection ratios of the transparent β-Ga_2O_3 photodetector at the two temperatures are calculated to be 7.8×10^5 and 9.8×10^5, respectively. To the best of our knowledge, these values rank among the highest reported for transparent photodetectors. The impressive rejection ratios emphasize the excellent UV spectral selectivity of the transparent β-Ga_2O_3 photodetector, and the high rejection ratio results from fewer defects in the films, which cause absorption and response in the visible light range. Meanwhile, the increase in responsivity with increasing operating temperature may be associated with the narrowing of the bandgap energy and the increase in the density-of-state distribution caused by lattice expansion at high temperatures.[48,49] The specific detectivity (D^*) is a crucial parameter for assessing the detection capability of a photodetector, which can be calculated by the following formula:[50,51]

$$D^* = \frac{R}{\sqrt{2qI_{\rm dark}/S}},$$

where R is the responsivity, q is the elementary charge, $I_{\rm dark}$ and S represent the dark current and the effective active area of the device, respectively. The specific detectivity of the photodetector in this work, using ITO electrodes at 25 °C, is calculated to be 1.3×10^{15} cm·Hz$^{1/2}$·W^{-1} (Jones) owing to its low dark current and high responsivity. The value demonstrates the device's exceptional capability for detecting weak light signals.

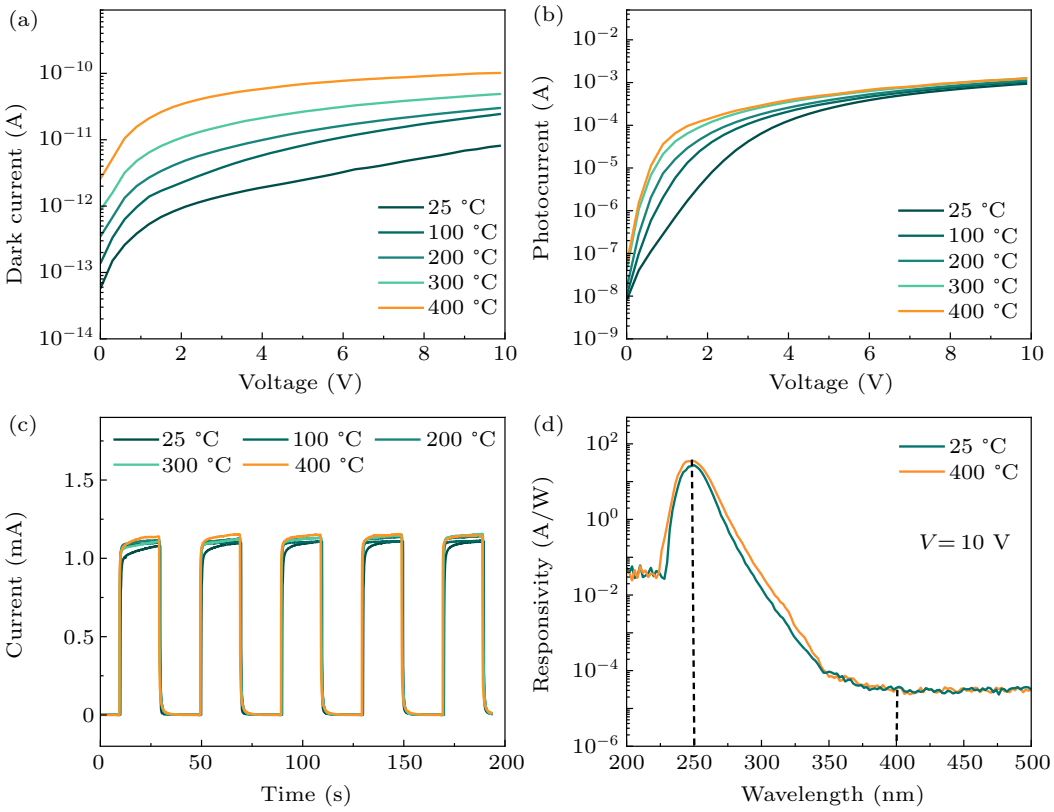


Fig. 5. The *I*–*V* characteristics (a) in the dark and (b) under 254 nm illumination at different temperatures. (c) Time-dependent current measured at different temperatures under 254 nm light and 10 V bias. (d) Spectral response plotted on a semilogarithmic scale at 25 °C and 400 °C under a 10 V bias.

4. Conclusion

In summary, we have demonstrated a high-performance visible transparent MSM solar-blind ultraviolet photodetector based on β-Ga_2O_3 films with stable crystalline ITO electrodes for application in transparent devices. The fabricated photodetector exhibits a low dark current of 7.5 pA, a large detectivity of 1.3×10^{15} Jones, and a superb UV/visible rejection ratio of 7.8×10^5, respectively. Meanwhile, the photodetector continues to maintain a highly sensitive, stable, and fast response even at elevated temperatures. Our work develops a fabrication strategy for high-performance transparent β-Ga_2O_3 solar-blind photodetectors, providing a path toward functional transparent electronics for extreme environment applications.

Acknowledgments

Project supported by the Natural Science Foundation of Jilin Province, China (Grant No. YDZJ202501ZYTS638) and the Fund of Education Department of Jilin Province (Grant Nos. JJKH20250694KJ and JJKH20250695KJ).

References

[1] Liu K, Sakurai M and Aono M 2010 *Sensors* **10** 8604
[2] Pearton S J, Yang J, Cary P H, Ren F, Kim J, Tadjer M J and Mastro M A 2018 *Appl. Phys. Rev.* **5** 011301
[3] Xie C, Lu X, Tong X, Zhang Z, Liang F, Liang L, Luo L and Wu Y 2019 *Adv. Funct. Mater.* **29** 1806006
[4] Yang J, Liu K, Chen X and Shen D 2022 *Prog. Quant. Electron.* **83** 100397
[5] Shu L, Yao S, Xi Z, Liu Z, Guo Y and Tang W 2024 *Nanotechnology* **35** 052001
[6] Cai Q, You H, Guo H, Wang J, Liu B, Xie Z, Chen D, Lu H, Zheng Y and Zhang R 2021 *Light Sci. Appl.* **10** 94
[7] Bosi M, Mazzolini P, Seravalli L and Fornari R 2020 *J. Mater. Chem. C* **8** 10975
[8] Fan M, Liu K, Chen X, Wang X, Zhang Z, Li B and Shen D 2015 *ACS Appl. Mater. Inter.* **7** 20600
[9] Liao M, Koide Y and Alvarez J 2006 *Appl. Phys. Lett.* **88** 033504
[10] Wu W, Huang H, Wang Y, Yin H, Han K, Zhao X, Feng X, Zeng Y, Zou Y, Hou X, Wei Z and Long S 2025 *J. Phys. D: Appl. Phys.* **58** 063003
[11] Kaur D and Kumar M 2021 *Adv. Opt. Mater.* **9** 2002160
[12] Zhu Y, Zhang D, Zheng W and Huang F 2020 *J. Phys. Chem. C* **124** 16722
[13] Xu J, Zheng W and Huang F 2019 *J. Mater. Chem. C* **7** 8753
[14] Zhang C, Liu K, Ai Q, Sun X, Chen X, Yang J, Zhu Y, Cheng Z, Li B, Liu L and Shen D 2023 *Mater. Today Phys.* **33** 101034
[15] Chen X, Ren F, Gu S and Ye J 2019 *Photonics Res.* **7** 381
[16] Guo D, Guo Q, Chen Z, Wu Z, Li P and Tang W 2019 *Mater. Today Phys.* **11** 100157
[17] Zhang C, Liu K, Ai Q, Huang X, Chen X, Zhu Y, Yang J, Cheng Z, Li B, Liu L and Shen D 2022 *J. Phys. Chem. C* **126** 21839
[18] Wang Y, Yang Z, Li H, Li S, Zhi Y, Yan Z, Huang X, Wei X, Tang W and Wu Z 2020 *ACS Appl. Mater. Interfaces* **12** 47714
[19] Yang L, Peng Y, Liu Z, Zhang M, Guo Y, Yang Y and Tang W 2023 *Chin. Phys. B* **32** 047301
[20] Qian L X, Gu Z, Huang X, Liu H, Lv Y, Feng Z and Zhang W 2021 *ACS Appl. Mater. Interfaces* **13** 40837
[21] Lin R, Zheng W, Zhang D, Zhang Z, Liao Q, Yang L and Huang F 2018 *ACS Appl. Mater. Interfaces* **10** 22419
[22] Li Z, Zhu R, Liang H, Su S and Mei Z 2025 *Chin. Phys. B* **34** 078502
[23] Wang B, Tang Z, Zheng H, Wang L, Wang Y, Wang R, Qiu Z and Zhu H 2023 *Chin. Phys. B* **32** 098508

[24] Tak B R, Garg M, Dewan S, Torres-Castanedo C G, Li K H, Gupta V, Li X and Singh R 2019 *J. Appl. Phys.* **125** 144501

[25] Zhou H, Cong L, Ma J, Chen M, Song D, Wang H, Li P, Li B, Xu H and Liu Y 2020 *J. Alloys Compd.* **847** 156536

[26] Wei T, Tsai D, Parvaneh R, Ke J, Tsai M, Lien D, Huang C, Horng R and He J 2014 *IEEE J. Sel. Top. Quantum Electron.* **20** 112

[27] Yang P K, Chang W Y, Teng P Y, Jeng S F, Lin S J, Chiu P W and He J H 2013 *Proc. IEEE* **101** 1732

[28] Kee S, Kim N, Park B, Kim B S, Hong S, Lee J H, Jeong S, Kim A, Jang S Y and Lee K 2018 *Adv. Mater.* **30** 1703437

[29] Wang L and Hu X 2020 *Batteries Supercaps* **3** 1275

[30] Chen D, Liu Z, Liang B, Wang X and Shen G 2012 *Nanoscale* **4** 3001

[31] Wu L, Fang H, Zheng C, Wang Q and Wang H 2019 *J. Mater. Chem. C* **7** 10446

[32] Park S H K, Hwang C S, Ryu M, Yang S, Byun C, Shin J, Lee J I, Lee K, Oh M S and Im S 2009 *Adv. Mater.* **21** 678

[33] Oukassi S, Baggetto L, Dubarry C, Le Van-Jodin L, Poncet S and Salot R 2019 *ACS Appl. Mater. Interfaces* **11** 683

[34] Kumar N, Arora K and Kumar M 2019 *J. Phys. D Appl. Phys.* **52** 335103

[35] Sui Y, Liang H, Huo W, Wang Y and Mei Z 2020 *J. Phys. D Appl. Phys.* **53** 504001

[36] Qiao B, Zhang Z, Xie X, Li B, Li K, Chen X, Zhao H, Liu K, Liu L and Shen D 2019 *J. Phys. Chem. C* **123** 18516

[37] Zhang X, Liu N, Lin H, Han D, Zhang W and Ye J 2025 *ACS Appl. Mater. Interfaces* **17** 17117

[38] Wang X, Cheng Z, Xu K, Tsang H K and Xu J B 2013 *Nat. Photon.* **7** 888

[39] Yu J, Lou J, Wang Z, Ji S, Chen J, Yu M, Peng B, Hu Y, Yuan L, Zhang Y and Jia R 2022 *J. Alloys Compd.* **872** 159508

[40] Gong X, Tong M, Xia Y, Cai W, Moon J S, Cao Y, Yu G, Shieh C-L, Nilsson B and Heeger A J 2009 *Science* **325** 1665

[41] Zhang Y, Wang Y, Fu R, Ma J, Xu H, Li B and Liu Y 2022 *J. Phys. D: Appl. Phys.* **55** 324002

[42] Yadav G, Gupta V and Tomar M 2021 *J. Mater. Res.* **37** 457

[43] Han D, Liu K, Yang J, Chen X, Li B, Liu L and Shen D 2021 *J. Mater. Chem. C* **9** 10013

[44] Zhang M, Ma W, Liu Z, Yang L, Li S, Guo Y and Tang W 2023 *Results Phys.* **54** 107110

[45] Liu H, Zhou S, Zhang H, Ye L, Xiong Y, Yu P, Li W, Yang X, Li H and Kong C 2022 *J. Phys. D Appl. Phys.* **55** 305104

[46] Cui S, Mei Z, Zhang Y, Liang H and Du X 2017 *Adv. Optical Mater.* **5** 1700454

[47] Ye L, Yu J, Mao Y, Xuan X, Pang D, Tang Y, Li H, Zhang H and Li W 2024 *Mater. Today Commun.* **40** 109665

[48] O'Donnell K P and Chen X 1991 *Appl. Phys. Lett.* **58** 2924

[49] Wang K and Reeber R R 1994 *Phys. Status Solidi A* **146** 621

[50] Luo X, Chen S, Liu L, Lv J, Qadir A, Shehzad K, Qiao X, Xu Y, Kienle L, Lotnyk A, Zhang X, Qian G and Fan X 2018 *J. Phys. Chem. C* **123** 810

[51] Zhang Y, Chen X, Xu Y, Ren F, Gu S, Zhang R, Zheng Y and Ye J 2019 *Chin. Phys. B* **28** 028501